Uncertainty quantification and sensitivity analysis of material parameters in crystal plasticity finite element models

M. Khadyko[1*], J. Sturdy[1], S. Dumoulin[2], L.R. Hellevik[1] and O.S. Hopperstad[1].

[1]*Department of Structural Engineering, Norwegian University of Science and Technology, NO-7491 Trondheim, Norway*

[2]*SINTEF Materials & Chemistry, NO-7465 Trondheim, Norway*

Abstract

A number of studies have directly compared measurements of polycrystals' deformation to the solution of a crystal plasticity model of the same polycrystal. An accurate representation of the full 3D microstructure and the boundary conditions has been shown to be important to obtain a good correspondence between the behaviour of the real and the simulated polycrystal. However, much less is known about the relationship between the global and the local solutions of crystal plasticity models and the influence of material parameters on the local response of the polycrystal. To address these questions, uncertainty quantification and sensitivity analysis are performed on finite element models of oligocrystals with a crystal plasticity material model. The results show significant variations in the simulated stress and strain fields due to variations in the material parameters. Sensitivity analysis is used to quantify the contribution of crystal orientation, latent hardening and other material model parameters to the variability of the crystal plasticity finite element model solution. The uncertainty in the stress and strain fields and their sensitivities vary between the oligocrystals, but nevertheless, some distinct trends can be identified. The most prominent trend is that, in general, the solution is most sensitive to the variations of the latent hardening description and the crystallographic orientations of the constituent crystals.

Keywords: crystal plasticity; finite element method; uncertainty quantification; sensitivity analysis; work-hardening.

1. Introduction

In the last decade, advances in both computational methods and experimental techniques have made it possible to create very detailed and precise finite element (FE) models of real

* Corresponding author (mikhail.khadyko@ntnu.no)

polycrystals and directly compare their simulated responses to experimental observations. Due to current computational limitations, the polycrystals studied are usually either very small [1-7], or their constituent grains are very big and few in number [8-14]. The small number of grains allows measuring and comparing the local strain fields on the surfaces of the specimens to the simulation results. Results from these kind of experimental studies may be used to calibrate single crystal plasticity (CP) models in a direct and consistent way, and are important for the modelling of localisation and fracture using crystal plasticity finite element methods (CP-FEM), which rely on the accuracy of the local solution of the stress and strain fields. Local measurements of strain fields in polycrystals may also reveal the influence of various microstructural features on the mechanical behaviour of the crystals, such as grain boundaries and inclusions.

The numerical aspects of this type of studies are examined in [15]. The role of mesh resolution, grain boundary representation and boundary conditions (BCs) is studied using a microstructure generated with a phase-field model. In [3, 5], simulations with realistic (obtained from the *in-situ* measurements with e.g. digital image correlation) and simplified BCs were compared, and realistic BCs were shown to be important for the accuracy of the simulation results. Another factor relevant for the accuracy of the predictions of the CP-FEM model is the real 3D microstructure, lying beneath the surface of the specimen, on which the strain measurements are performed. In [3, 4, 16], it was demonstrated that it is not possible to accurately predict the strain field on the surface of a specimen with significant thickness without accounting for the whole structure.

The role of the CP model parameters has only been studied briefly. In [7], the way the grain orientations are assigned to the elements of the CP-FEM model was studied. The most often used method is assigning the average orientation to all elements within one grain, which was compared to assigning a locally measured orientation to each corresponding element. The relative influence of work-hardening parameters and BCs was compared in [5]. Yet to the best of the authors' knowledge, no extensive quantitative studies of the sensitivity of the local CP-FEM solutions to the parameters of the constitutive model have been performed. The CP model parameters are usually obtained by comparing the simulated and experimental force-displacement curves. In the fitting procedure, the material parameters are either chosen based on previous studies (usually the case with the latent hardening description), varied within some physically plausible range (as with the dislocation accumulation and annihilation terms in the Kocks-Mecking type models [17]), or varied more or less arbitrary (as for the

parameters of the Pierce-Asaro-Needleman model [18]). One caveat when using such methods is that different sets of parameters may result in similar global force-displacement responses but different local solutions [19]. To address this possibility, the investigation in [2] attempted to use both the local and global response of the polycrystal in the fitting procedure and found that obtaining a set of parameters that satisfies both the global force-displacement curve and the local strain field equally well was not possible. Given these limitations, it is desirable to assess the impact of the uncertainty in the CP model parameters through the mathematical framework of uncertainty quantification (UQ) and sensitivity analysis (SA). UQ can quantify the variability of model predictions for given uncertainty about model parameters, while SA evaluates how individual parameters contribute to this variability.

The perspective of UQSA views a computational model as a function that relates inputs, $\mathbf{z}$, to outputs or quantities of interest $y = f(\mathbf{z})$. However, instead of treating $\mathbf{z}$ as exactly known, the uncertainty about input values is accounted for by treating them as random variables with a probability distribution that represents the likelihood or plausibility of different values of the inputs, e.g. if an input is known only to be bounded between two values it may be represented as a uniform random variable. Thus the output of the model is not a single deterministic value but a random variable with a probability distribution that may be analysed to quantify the uncertainty and further the contribution of individual inputs to that uncertainty may be quantified by sensitivity analysis.

Various UQ and SA tools have been applied in a wide range of scientific fields including structural analysis [20], hydrology [21], environmental engineering [22], biomechanics and many more. An overview and guide to the application of UQSA methods may be found in [23]. The methods themselves are not specific to any particular field and may be applied to analyse any kind of model relating uncertain inputs to uncertain outputs. For example a parametric study of the phenomenological plasticity and fracture models was performed in [24].

The main focus of the UQ studies in crystal plasticity has been the variability of the microstructure (grain morphology and crystallographic texture) and the material processing parameters and their influence on the global response of the polycrystalline materials. A number of studies have been performed by Zabaras and co-authors [25-27]. These studies develop a methodology, summarized in [28], which reduces the complexity of a polycrystals' microstructure to a set of functions, which may be treated by the UQ methods. The

propagation of uncertainty from the microstructure to the global response of the material is a topic of several other studies [29-32]. A review of the UQSA methods applied in material science [33] suggests that this field is still in its nascent stage.

Some attempts to assess the sensitivity of the CP-FEM solution to e.g. uncertainty in the latent hardening matrix were made in [34, 35]. In both studies, each independent component of the matrix was assigned a high value, while all others were held at unity. Then the response of the model for all cases was qualitatively compared. This is a local form of UQSA. Local methods examine the effect of a change around a reference value for one model input while keeping all other inputs fixed. In many cases the dependency of the output on the input parameters may be non-additive, non-monotonic, and non-linear, at least in some locations of the input space. Therefore the results obtained by local methods could be misleading as these effects will not be reflected by the local analysis. Global methods consider the whole input space and can account for non-additive, non-monotonic, and non-linear dependencies of the output on the input and are thus in general more reliable and informative than local methods.

Global methods of UQSA can be categorized as intrusive or non-intrusive. Intrusive approaches require the uncertainty in the model inputs to be substituted into the model to derive new governing equations accounting for uncertainty. On the other hand, non-intrusive methods do not require modification of the existing models. Model outcomes are obtained using the usual (deterministic) solver for a set of different input samples. UQSA is then based on the outputs obtained for each input sample. This approach can be applied to any model with any numerical implementation, and it is therefore much better suited for the present study. In this work the polynomial chaos (PC) method [36] is used. The method consists of the following steps:

1. Identification of the outputs of interest (in our case some way of representing the stress and strain fields as a convenient set of values is necessary),
2. Identification and assessment of the distribution of the uncertain inputs (in our case the uncertain inputs are the material model parameters and their distribution should be chosen),
3. Sampling of the input space to acquire samples (i.e., discrete sets of material parameters should be picked from the chosen distribution),

4. Evaluation of the deterministic model to obtain the outputs, corresponding to the inputs from the previous step (i.e., CP-FEM simulations with the sampled sets of material parameters are performed),
5. Calculation of UQSA measures,
6. Assessment of convergence of UQSA measures.

A more detailed overview of the methods may be found in [23].

As the appropriate values of material parameters for a given CP-FEM model are generally quite uncertain, this study investigates the resulting uncertainty of the stress and strain fields of a CP-FEM solution due to the uncertainty in the material parameters. Additionally, sensitivity analysis investigates the relative contributions of each material parameter. The subject of UQSA is a set of 2D and 3D oligocrystals subjected to uniaxial tensile loading. The UQSA method allows performing a global quantitative analysis of the said uncertainties and sensitivities, unlike the local qualitative studies previously performed with CP-FEM. In addition to improving understanding of the effects of material parameters in CP-FEM simulations, the article also aims more broadly to introduce the aforementioned UQSA methods and tools into CP-FEM.

2. Uncertainty quantification and sensitivity analysis

To account for the uncertainty about parameters they are treated as a random vector, $\mathbf{Z}$, where the probability distribution of $\mathbf{Z}$ represents the likelihood or plausibility of different values of the input. Thus the quantity of interest is a random variable defined by applying the function to the random variable $\mathbf{Z}$, i.e., $Y = f(\mathbf{Z})$.[†] The uncertainty about the quantity of interest may be quantified by the expected value and variance of Y

$$\mathrm{E}(Y) = \int_{-\infty}^{\infty} y \rho_Y(y)\, dy, \quad \mathrm{Var}(Y) = \int_{-\infty}^{\infty} \{y - \mathrm{E}(Y)\}^2 \rho_Y(y)\, dy \tag{1}$$

where $\rho_Y(y)$ is simply the probability density function of Y.

Beyond accounting for the inherent uncertainty about the model prediction, sensitivity analysis (SA) can determine the contribution of particular components of $\mathbf{Z}$, i.e., specific

[†] Note that deterministic or known values are traditionally denoted with lowercase letters, while uppercase letters represent random variables. Values realized from the random variable $\mathbf{Z}$ or specific points within the range of $\mathbf{Z}$ are denoted by $\mathbf{z}$ as their values are known and have no uncertainty.

inputs, to the uncertainty of Y . Variance based sensitivity analysis decomposes the variance of the model output, $\mathrm{Var}(Y)$, into portions attributable to specific inputs or combinations of inputs. There are two widely used sensitivity indices based on this decomposition of variance. The first is called the first order or main sensitivity index of input Z_i and is given by

$$S_{M,i} = \frac{\mathrm{Var}\{\mathrm{E}(Y \mid Z_i)\}}{\mathrm{Var}(Y)}. \tag{2}$$

This index measures the fraction of total variance that is attributable to variability of Z_i independent of the variability of all other inputs and if Z_i were known exactly the $\mathrm{Var}(Y)$ would be expected to decrease by that proportion. The main sensitivity index $S_{M,i}$ is useful for prioritizing which parameters may be most influential on the model behaviour as a large value indicates that changes in Z_i alone have significant impacts on the model output. The second index is called the total sensitivity index of input Z_i and is defined as

$$S_{T,i} = \frac{\mathrm{E}\{\mathrm{Var}(Y \mid \mathbf{Z}_{\neg i})\}}{\mathrm{Var}(Y)} \tag{3}$$

where $\mathbf{Z}_{\neg i}$ is the vector of all inputs except Z_i. This index measures the expected amount of variability remaining if all other variables except Z_i were known exactly. It may be useful for identifying irrelevant parameters as a low value of $S_{T,i}$ suggests that Z_i is not an influential input on the model output, and conversely measurements of Y do not provide significant information about Z_i in the context of parameter estimation and design of experiments, e.g. [37]. Thus sensitivity indices may also be used to identify the viability of estimating parameters from particular measurements.

The case where the first order index is quite small while the total index is large indicates that the parameter has strong interactive effects. In other words, the parameter's influence is largely dependent on the values of other parameters, thus the effect of changing its value alone may cause very different responses. For example, a parameter may be important in a component of the model that is activated only for certain levels of other parameters.

A number of methods may be employed to characterize $Y = f(\mathbf{Z})$ or its probability distribution such as Monte Carlo methods or modifying the governing equations to solve the

stochastic problem directly [23]. In this study we use a nonintrusive method[‡] called polynomial chaos which represents the function $f(\mathbf{z})$ as a series of orthogonal polynomials

$$f_N(\mathbf{z}) = \sum_{i=0}^{k(N)} c_i \Phi_i(\mathbf{z}), \qquad k = \binom{D+N}{N} = \frac{(D+N)!}{N!D!} \tag{4}$$

where N denotes the highest order polynomial, k denotes the number of terms, and D is the number of components in $\mathbf{Z}$. The basis polynomials are chosen to be orthogonal with respect to the probability density $\rho_{\mathbf{Z}}(\mathbf{z})$ of $\mathbf{Z}$ such that

$$\int_{-\infty}^{\infty} \Phi_i(\mathbf{z}) \Phi_j(\mathbf{z}) \rho_{\mathbf{Z}}(\mathbf{z}) d\mathbf{z} = \mathrm{E}\left(\Phi_i(\mathbf{Z}) \Phi_j(\mathbf{Z})\right) = \gamma_i \delta_{ij} \quad (\text{no sum}) \tag{5}$$

where E is the expected value, γ_i is a normalisation constant associated with Φ_i, and δ_{ij} is the Kronecker delta. This orthogonality ensures that the probabilistic moments of $Y_N = f_N(\mathbf{Z})$ are simply algebraic combinations of the coefficients, c_i, and thus once the coefficients are obtained the expected value, variance, and sensitivity indices are easily calculated. To evaluate the coefficients a linear least squares problem is formulated by evaluating the model at a number of different points in the parameter space sampled according to the probability distribution of $\mathbf{Z}$ and the output values are regressed on the basis functions. The convergence rate of $Y_N = f_N(\mathbf{Z})$ with respect to the maximum order N is dependent on the smoothness of $f(\mathbf{z})$, but typically only order 4 or 5 is sufficient to achieve converged and accurate estimates of expected value, variance and sensitivity indices. This must be checked by verifying that the estimates are consistent between successive orders of approximation. In this study, it was ensured that the UQSA measures calculated from $f_N(\mathbf{Z})$ and $f_{N-1}(\mathbf{Z})$ have a relative precision within 1%.

In this study the Python package *chaospy* [38] is employed to sample from the distribution of $\mathbf{Z}$, generate basis polynomials for specified orders of truncation, solve the regression problem and finally evaluate the variability and sensitivity indices.

[‡] Nonintrusive means that the underlying deterministic model does not need to be modified.

3. Numerical models

3.1. Single crystal plasticity model

The single crystal plasticity model used in this work is formulated within a finite deformation framework. The total deformation gradient $\mathbf{F}$ is multiplicatively decomposed as [18]

$$\mathbf{F} = \mathbf{F}^e \mathbf{F}^p \tag{6}$$

where $\mathbf{F}^e$ and $\mathbf{F}^p$ are the elastic and plastic part of $\mathbf{F}$, respectively. The plastic part $\mathbf{F}^p$ transforms the body from the initial to the intermediate configuration by plastic slip, whereas the elastic part $\mathbf{F}^e$ transforms the body from the intermediate to the current configuration by elastic deformation and rigid body rotation. The plastic velocity gradient $\bar{\mathbf{L}}^p$ on the intermediate configuration is defined by

$$\bar{\mathbf{L}}^p = \dot{\mathbf{F}}^p \left(\mathbf{F}^p\right)^{-1} = \sum_{\alpha=1}^{n} \dot{\gamma}^\alpha \mathbf{m}_0^\alpha \otimes \mathbf{n}_0^\alpha \tag{7}$$

where the orthonormal vectors $\mathbf{m}_0^\alpha$ and $\mathbf{n}_0^\alpha$ are the slip direction and slip plane normal vectors, respectively, for a slip system α in the initial and intermediate configurations, $\dot{\gamma}^\alpha$ is the slip rate on slip system α, and n is the total number of slip systems.

The elastic Green strain tensor $\bar{\mathbf{E}}^e$ defined with respect to the intermediate configuration is given by

$$\bar{\mathbf{E}}^e = \frac{1}{2}\left(\bar{\mathbf{C}}^e - \mathbf{I}\right), \quad \bar{\mathbf{C}}^e = \left(\mathbf{F}^e\right)^T \mathbf{F}^e \tag{8}$$

where $\bar{\mathbf{C}}^e$ is the elastic right Cauchy-Green deformation tensor and $\mathbf{I}$ is the second-order unity tensor. The second Piola-Kirchhoff stress tensor $\bar{\mathbf{S}}$ on the intermediate configuration reads as

$$\bar{\mathbf{S}} = J \left(\mathbf{F}^e\right)^{-1} \boldsymbol{\sigma} \left(\mathbf{F}^e\right)^{-T} \tag{9}$$

where $\boldsymbol{\sigma}$ is the Cauchy stress tensor and $J = \det \mathbf{F}$ is the Jacobian determinant. A linear hyperelastic relation for small elastic strains is defined by

$$\bar{\mathbf{S}} = \bar{\mathbf{C}}_{el}^{\bar{S}} : \bar{\mathbf{E}}^e \tag{10}$$

where $\overline{\mathbf{C}}_{el}^{\overline{S}}$ is the fourth order tensor of elastic moduli. For the FCC lattice, on which this study focuses, this tensor has three independent components describing the elastic anisotropy of the crystal.

The plastic flow is described by [39]

$$\dot{\gamma}^{\alpha} = \dot{\gamma}_0 \left(\frac{\left| \tau^{\alpha} \right|}{\tau_c^{\alpha}} \right)^{\frac{1}{m}} \operatorname{sgn}\left(\tau^{\alpha} \right) \tag{11}$$

where $\dot{\gamma}_0$ is the reference slip rate, m is the instantaneous strain rate sensitivity, τ_c^{α} is the yield strength of slip system α, and the resolved shear stress τ^{α} is obtained as

$$\tau^{\alpha} = \overline{\mathbf{C}}^{e} \overline{\mathbf{S}} : \left(\mathbf{m}_0^{\alpha} \otimes \mathbf{n}_0^{\alpha} \right) \tag{12}$$

The hardening is defined by

$$\dot{\tau}_c^{\alpha} = \theta(\Gamma) \sum_{\beta=1}^{n} q_{\alpha\beta} \left| \dot{\gamma}^{\beta} \right| \tag{13}$$

where $\theta(\Gamma)$ is the master hardening modulus, $q_{\alpha\beta}$ is the matrix of self-hardening and latent-hardening coefficients, and the accumulated slip Γ is defined by the evolution equation

$$\dot{\Gamma} = \sum_{\alpha=1}^{n} \left| \dot{\gamma}^{\alpha} \right| \tag{14}$$

The master hardening modulus $\theta(\Gamma)$ is defined as [40]

$$\theta(\Gamma) = \theta_1 + \left(\theta_0 - \theta_1 + \frac{\theta_0 \theta_1}{\tau_1} \Gamma \right) \exp\left(-\frac{\theta_0}{\tau_1} \Gamma \right) \tag{15}$$

where θ_0, θ_1 and τ_1 are material parameters. The initial slip resistance τ_0 is assumed equal for all slip systems.

The crystal plasticity material model was implemented as a user-material subroutine, using the explicit integration scheme by Grujicic and Batchu [41].

3.2. CP-FEM models

Investigating the effects of uncertainty about CP model parameters requires considering microstructure models that satisfy several constraints. The models should be generic enough such that the results obtained are representative of a range of similar models. Further, the models should be small enough to make running a multitude of simulations feasible. The models should also include enough grains to provide a wide range of interactions between the grains and the resulting inhomogeneous stress and strain fields. Finally, the meshes must be fine enough to resolve these fields in detail yet coarse enough for a fast and efficient simulation.

Therefore the morphology chosen for the study was a generic Voronoi tessellation type structure with ten approximately equiaxed convex grains representing oligocrystals. Both a 2D structure with plane-strain conditions and a 3D structure were used. The structures are shown in Figure 1. The model was subjected to tension by applying a velocity along the *x*-axis to its right edge (or face in case of 3D model) which smoothly ramps up to a constant value. The left edge (or face) of the model is constrained in displacement in the *x*-direction and the other edges (faces) are free. The effect of BCs on the local stress and strain fields in polycrystals was studied elsewhere [3, 5]. To explore different configurations and interactions of hard/soft orientations, 5 different sets of 10 random crystallographic orientations were assigned to the 10 grains of the 2D and 3D models. This provided 5 models with markedly different stress and strain fields on which the sensitivities could be calculated and compared.

The mesh of the 2D CP-FEM model consists of 3004 two-dimensional plane-strain elements, and that of the 3D model consists of 8000 brick elements. Reduced integration and the Flanagan-Belytschko stiffness-based hourglass control [42] were used in both cases. The explicit solver of the nonlinear FEM code LS-DYNA [43] was used in the calculations. Mass-scaling was applied to reduce the computation time and the kinetic energy was controlled at every step to ensure that it was very small compared to the total energy and that the simulation remained quasi-static.

3.3. Distribution of material parameters

In this study, aluminium is used as a model material. The material parameters are therefore based on the parameters of Al alloys studied previously in [44]. The baseline values and ranges of the material parameters are summarized in Table 1.

The elastic constants depend on the interatomic potentials, are similar in all Al alloys, and may be measured with high accuracy. Thus, the elastic constants were excluded from the sensitivity study. Crystal plasticity simulations and experiments are often limited to quasi-static cases (very low strain rates), for which rate-independent and rate-dependent single crystal plasticity models produce identical results [45, 46]. The choice of the reference slip rate $\dot{\gamma}_0$ and the rate sensitivity m does not affect the solution as long as m is sufficiently small to preserve rate-insensitivity. Thus these parameters were also excluded from the sensitivity study. The values used for the elasticity constants and the constants governing rate dependence are summarized in Table 2.

The Euler angles describing the orientation of the crystal are parameters that do not appear explicitly in the material model, but are nevertheless crucial. In this work, the Euler angles are defined following the conventions established in [47]. The crystal orientations are usually measured by EBSD on a grid covering a patch of a polycrystal. Errors in the measurements may introduce various sources of random and systematic errors to the orientation. In CP-FEM models, orientations are most often assigned by finding the average of the orientations measured within a crystalline grain and assigning the resulting orientation to all elements within this grain. An alternative approach uses the grid points of the EBSD scan as the centroids of the elements of the CP-FEM model and assigns the orientation measured in each point to the corresponding element. The first approach is the most widespread in CP-FEM models, thus it is utilized in this study. The first Euler angle φ_1 (i.e., the rotation around the *z*-axis according to the coordinate system defined in Figure 1) is assumed to vary around the base value within a ±2° range for all the grains in the model. This may be e.g. representing the error of the specimen positioning in the electronic microscope, or other systematic error.

The next group of parameters includes the initial slip resistance τ_0 and the hardening parameters θ_0, θ_1 and τ_1. These parameters do not have a direct physical connection to the microstructure of the material and can only be derived indirectly from the force-displacement curve and the deformation of the specimen. Considering all the errors associated with experimental and numerical procedures, these parameters are highly uncertain. In this work, we use two different baseline sets of the initial slip resistance and the hardening parameters. One represents a ductile alloy reinforced mainly by solid solution of the alloying elements, with values corresponding to AA6063-T4, and the other represents a stronger but less ductile

alloy reinforced mainly by precipitate particles, with values corresponding to AA6063-T7 [44]. The material parameters are assumed to vary within a range of ±30% of the baseline value.

The next parameter is the latent hardening coefficient q. This parameter is very difficult to evaluate experimentally, so its value is based on the estimations provided by e.g. [48, 49] or some geometrical arguments [50]. Quite often, it is assumed for simplicity to be unity (i.e., latent hardening equals self-hardening), as in [51]. The most common value used in CP-FEM simulations is $q = 1.4$, though $q = 1.6$ was also proposed by [48]. In this work, it is assumed that the latent hardening of the crystal can be described by the latent hardening matrix with one independent parameter, and that the most correct value of this parameter is within the range $q \in [1, 2]$ with $q = 1.5$ as the baseline value.

3.4. Identification of the outputs of interest

Simulations with material parameters lying in the centre of the respective ranges (see Table 1) are used as a baseline to which all other simulations are compared by computing the normalized root mean squared deviation (RMSD) of the scalar field variable ϕ, defined by

$$\mathrm{RMSD}(\phi) = \sqrt{\frac{1}{N_e}\sum_{n=1}^{N_e}\left(\frac{\phi_n}{\tilde{\phi}} - \frac{\phi_{0n}}{\tilde{\phi}_0}\right)^2} \tag{16}$$

where the local value ϕ_n of the variable ϕ is obtained in the n^{th} element of the N_e elements of the model, $\tilde{\phi}$ is a normalization factor calculated from the field ϕ. Further, ϕ_0 represents the baseline field and $\tilde{\phi}_0$ the corresponding normalization factor. The particular normalization values $\tilde{\phi}$ and $\tilde{\phi}_0$ used for each scalar field are discussed below. Note that RMSD is identical to root mean squared error, but in this case there is no error per se rather just a metric of the average deviation over the mesh.

The first scalar field variable is the equivalent plastic strain field, ε^p, conjugate with the von Mises norm of the stress field. The value of the equivalent plastic strain ε^p is calculated in each element of the model at different points of the deformation history (at approximately 5%, 10% and 15% global strain). Then, the field produced by the model with varied material parameters is compared to the field produced by the baseline simulation. In this case, ϕ is the equivalent plastic strain ε^p; ϕ_n and ϕ_{0n} are the equivalent plastic strains in the n^{th} element of

the current and the baseline simulation, respectively; $\tilde{\phi}$ and $\tilde{\phi}_0$ are both the global strain (which should be equal to the average of the strain for all elements in this case and also identical for all simulations including the baseline). The $\mathrm{RMSD}(\varepsilon^p)$ is a non-negative scalar that shows how much the normalized strain field in the current simulation with the current set of material parameters differs from the normalized strain field in the baseline case. Minimization of this or a similar function may be used in a material parameters identification procedure, as e.g. in [2].

The second field is the equivalent (von Mises) stress field, here denoted σ. Whereas the average plastic strain in all simulations was identical, the average stress varied greatly and depends strongly on the yield strength and work-hardening. In this case, ϕ is the equivalent stress σ; ϕ_n and $\tilde{\phi}$ are the equivalent stress in the n^{th} element and average equivalent stress in the current simulation; ϕ_{0n} and $\tilde{\phi}_0$ are the corresponding quantities for the baseline simulation. The third and fourth scalar fields applied in the sensitivity study are the hydrostatic pressure field P and the stress triaxiality field $T = -P/\sigma$. The RMSD of these fields is calculated in the same manner as for the equivalent stress field.

The final target of the sensitivity study is the global force-displacement curve. This curve is often used for the material parameter fitting, and as mentioned before, it was used alongside the local strain field for this purpose in [2] with little success. A typical fitting procedure would minimize the squared error between the experimental and the simulated force-displacement curve by varying the material parameters. Here the same type of measure is applied. The baseline curve is again used as reference (or provisional "experimental" curve) and the RMSD is defined by

$$\mathrm{RMSD}(F) = \sqrt{\frac{1}{N_d}\sum_{i=1}^{N_d}\left(\frac{F(d_i) - F_0(d_i)}{F_0(d_i)}\right)^2} \tag{17}$$

where $F(d)$ is the total force at displacement d in the current simulation, $F_0(d)$ is the corresponding force in the baseline simulation, N_d is the number of simulation history points where the force and displacement are obtained, and d_{N_d} is the maximum displacement.

3.5. Evaluation of polynomial chaos expansions and UQSA measures

To understand how much the variability of the parameters, denoted by the vector $\mathbf{Z} = \left(\Delta\varphi_1 \quad \tau_0 \quad \tau_1 \quad \theta_0 \quad \theta_1 \quad q\right)$, influences CP-FEM simulations, UQSA of the outputs of interests was performed for each of the configurations discussed in Section 3.2. As no statistical evidence was available to characterize the distribution of the parameters considered, each parameter was described as an independent uniform random variable with ranges given in Table 1, i.e., all values in the range are treated as equally valid.

UQSA for each configuration was performed by employing the *chaospy* software package [38] to generate samples in the input space and basis polynomials, to estimate coefficients of the expansion based on a linear regression of the output value, and finally to estimate measures of uncertainty and sensitivity indices.

For each material type (T4 and T7), a set of sample values was generated according to the Hammersley quasi-random sequence [52], as this sequence is nested and allows for successively increasing the number of points in the quasi-random sequence by only evaluating the number of additional samples required. The maximum polynomial order was $N = 5$, which requires estimating $k = 462$ coefficients, and thus 924 samples (simulations) for the chosen regression method. This order was chosen to ensure that the estimates of sensitivity indices agreed within 1% between successive orders of polynomials.

Evaluation of the CP-FEM models for each input sample was performed as described in Section 3.2, followed by post processing of each simulation to calculate the outputs of interest (see Section 3.4) corresponding to each input sample. For each post-processed output, the coefficients of a truncated polynomial expansion were estimated by the regression method, and subsequently the expected value, variance, standard deviation, and sensitivity indices were calculated from the coefficients.

3.6. Averaging of results across orientations

As discussed in Section 3.1, this analysis considered CP-FEM models based on two generic structures (one 2D and the other 3D as shown in Figure 1). Applying 5 unique combinations of crystallographic orientations to each of these generic structures generated 5 CP-FEM models for both 2D and 3D simulations. For each of these 5 models, uncertainty quantification and sensitivity analysis were conducted once over the range of T4 material parameters and again over the range of T7 material parameters. Thus, uncertainty and

sensitivity measures were estimated for 20 distinct cases, i.e., 5 cases for each of 2D-T4, 2D-T7, 3D-T4, and 3D-T7 models.

As the exact sensitivities and uncertainties generally depend on the specific CP-FEM model, the goals of this UQSA were to investigate: (1) how much the quantities outlined in Section 3.2 vary on average over the range of material parameters, (2) if model sensitivities are consistent over the range of crystallographic orientations and structures, and (3) which, if any, parameters are consistently more influential on these quantities. As such, it was necessary to combine and summarize the UQSA results by averaging the results from each of the individual analyses conducted as well as calculating meaningful measures of the variability of these quantities across crystallographic orientations.

In this analysis RMSDs quantified the deviation of global force, equivalent plastic strain, equivalent stress, hydrostatic pressure, and stress triaxiality from a reference value calculated based on the average value of all parameters. This measure provides a convenient measure of the deviation of the model solution from the baseline solution at nominal parameter values. The UQ estimates the expected value and standard deviation of the RMSDs for a given set of crystallographic orientations. The expected values of the RMSDs measure how much the quantities of interest differ on average from the reference values. The standard deviation of the RMSDs quantifies the spread of these deviations over the possible parameter values, i.e., a low standard deviation suggests that most possible parameter sets produce values deviating from the reference values to a similar extent, whereas a large standard deviation of the RMSDs suggests that there are quite different levels of deviation for distinct points in the parameter space. To compare both of these aspects across sets of crystallographic orientations, the average value of the expected RMSDs as well as the average value of the standard deviation of RMSDs across all orientation sets within each group (2D-T4, 2D-T7, 3D-T4, and 3D-T7) were calculated. For each quantity of interest (see Section 3.2), the average RMSD and its associated average standard deviation are reported as

$$\overline{E(X)} \pm \overline{\mathrm{std}(X)} = \frac{1}{n}\sum_{i=1}^{n} E(X_i) \pm \frac{1}{n}\sum_{i=1}^{n} \mathrm{std}(X_i) \tag{18}$$

where n is the number of sets of crystallographic orientations, X denotes the RMSD of one of the mechanical fields analysed, and X_i denotes the RMSD of the same field calculated for the i^{th} set of crystallographic orientations.

To summarize the sensitivity analyses for various sets of crystallographic orientations, the average value, $\overline{S}_j$, and sample standard deviation, $s(S_j)$, of each sensitivity index over all sets of crystallographic orientations for a given material and geometry were calculated as

$$\overline{S}_j = \frac{1}{n}\sum_{i=1}^{n} S_{j,i}, \quad s(S_j) = \sqrt{\frac{1}{n}\sum_{i=1}^{n}\left(S_{j,i} - \overline{S}_j\right)^2} \tag{19}$$

where j indicates a specific parameter and i indexes the sets of crystallographic orientations.

4. Results and discussion

The UQ results for the RMSDs are presented in Figure 2 against the global strain level. The RMSD for most of the fields naturally tends to increase with strain, though in some models it remains almost constant.

The RMSD of the global force is almost constant and independent of the strain level. For both the 2D and 3D models and for both materials, the average is around 12% with an average standard deviation of 6%. The maximum variation in the force is illustrated by the engineering stress-strain plots for one orientation set for each model type in Figure 3. The plots show the baseline simulation curve as well as the curves with the highest $RMSD(F)$, i.e., the engineering stress-strain curves for all other simulations lie within the area bounded by these two curves. The plot may be compared to the results of the uniaxial tension tests in [44]. The material in [44] is extruded and possesses a strong crystallographic texture, therefore its response cannot be directly compared to the response of the model olygocrystals. Nevertheless, the yielding and work-hardening behaviour of the oligocrystals is still quite similar to the results in [44].

In the 2D models, the highest average value and average standard deviation are found for $\mathrm{RMSD}(\varepsilon^p)$. In particular, the average value of $\mathrm{RMSD}(\varepsilon^p)$ reaches 15% for the T4 material and over 40% for the T7 material, meaning that choosing arbitrary values of material parameters from the nominal ranges results in the level of strain in each element on average differing by 15% and 40%, respectively, from the baseline value in the two cases. The variability of $\mathrm{RMSD}(\varepsilon^p)$ for the T7 material is also high, reaching 15% at higher strains, indicating that the plastic strain fields obtained from different material parameter sets are not only different from the baseline, but also from each other. The high $\mathrm{RMSD}(\varepsilon^p)$ for the T7 material is most likely due to its low work-hardening and tendency to localize. The exact

position of localization may change, creating large differences between the current and the baseline plastic strain fields. For the T4 material, the plastic strain field is more homogeneous, giving a lower $\mathrm{RMSD}(\varepsilon^p)$.

For the 3D models, $\mathrm{RMSD}(\varepsilon^p)$ is much smaller, just below 5% for the T4 material and just above 5% for the T7 material. The average variabilities for the 3D models are also small, on the order of 2-3%. Considering that the material model is the same, the difference stems from the plane-strain condition and more constrained plastic flow in the 2D model, which makes it more prone to plastic instability and localization. To illustrate the described trends, a collection of equivalent plastic strain contour plots are presented in Figure 4 on the deformed configuration. The equivalent strain contour plots show the baseline simulation and the simulation with the highest $\mathrm{RMSD}(\varepsilon^p)$ for one of the orientation sets.

The equivalent stress field is very stable, with both low average $\mathrm{RMSD}(\sigma)$ and low average variability, independent of the model and material type. The average $\mathrm{RMSD}(\sigma)$ is less than or equal to around 5%. The RMSDs for the hydrostatic pressure field and the stress triaxiality field show very similar average values and variabilities. This is not surprising when considering the definition of the stress triaxiality and the low RMSD of the von Mises stress. The average values of $\mathrm{RMSD}(P)$ and $\mathrm{RMSD}(T)$ for the 2D models are 10% for the T4 material and 15% for the T7 material. Notably, the dependence of the RMSDs on material type is reversed for the 3D model, where the average is almost 20% for the T4 material and 15% for the T7. The variability of the RMSDs for the hydrostatic pressure and stress triaxiality is also fairly consistent for all models and is around 5%. These trends may have some consequences in the CP-FEM modelling of ductile fracture. The low variability of the stress field shows that it is possible to obtain a good estimate of the equivalent stress distribution in the oligocrystal even when the material parameters are not known precisely. On the other hand, the stress triaxiality estimation requires a higher accuracy of the estimation of the material parameters.

Calibrating material model parameters based on force-displacement curves raises the question of whether there is a correlation between the RMSD of the force and the plastic strain field. If these quantities vary independently of each other, the correlation will be negligible, and the best fit for the force-displacement curve does not necessarily produce the best fit for the plastic strain field. On the other hand, if there is a correlation, then a better fit of the force-

displacement curve should produce a model with better predictions of the local strain field. The correlations of $\mathrm{RMSD}(F)$ and $\mathrm{RMSD}(\varepsilon^p)$ for each set of crystallographic orientations were calculated by

$$\mathrm{corr}(x, y) = \frac{\sum_{i=1}^{n}(x_i - \bar{x})(y_i - \bar{y})}{\sqrt{\sum_{i=1}^{n}(x_i - \bar{x})^2 \sum_{i=1}^{n}(y_i - \bar{y})^2}} \tag{20}$$

with $x = \mathrm{RMSD}(F)$ and $y = \mathrm{RMSD}(\varepsilon^p)$, $\bar{x}$ and $\bar{y}$ denote the average values of the RMSD for the $n = 928$ simulations of the given set of crystallographic orientations. For each material type the average correlations and their associated standard deviations were also calculated in the same manner as those of the sensitivity indices (19). The resulting values are presented in Figure 5. The correlation coefficients are small in all cases, although they are higher for the 3D models than for the 2D models. Even the highest values are just around 30%. Thus, in the case of the models and orientation sets tested, the force and the strain field varied mostly independently of each other.

The sensitivity indices for the global force are presented in Figure 6. Both 2D and 3D models demonstrate similar trends. In all cases, $\mathrm{RMSD}(F)$ is most sensitive to the initial slip resistance τ_0. The main sensitivity indices for all other material parameters are negligible. On the other hand, the total sensitivity indices for the T4 material for both the 2D and 3D models are increasing with strain and become significant for q, τ_1 and θ_0. For the T7 material, the total sensitivities are still negligible for these parameters. Both the main and total sensitivity indices of θ_1 and $\Delta\varphi_1$ are negligible for all models and material types. The trend seen for the total sensitivities is likely the result of the different work-hardening of the T4 and T7 materials. The T4 material has significant work-hardening so the force level has more room for variation, in contrast to the T7 material for which the force level can only moderately deviate from the force at yielding. The work-hardening parameters primarily affect $\mathrm{RMSD}(F)$ only in interaction with each other, as only their total sensitivity indices are significant, while their main sensitivity indices remain negligible. In other words, the effect of the work-hardening parameters is highly dependent on the values of the other parameters. For some values of other parameters they may have high influence, but on average they have no strong independent effect. If the force-displacement curve is used for the material model calibration, then for the T7 material only the initial slip resistance may be determined with

certainty, the other parameters do not affect it noticeably within the given ranges. On the other hand, the local fields show very different sensitivities. A conclusion can be made, that for low work-hardening alloys it is not possible to establish the local material parameters of the CP model, based on the global stress-strain curve. In contrast, the calibration of the material model to the force-displacement curve of T4 material allows adjusting the initial slip resistance as well as the hardening parameters, particularly for larger displacements.

The sensitivity indices for $\mathrm{RMSD}(\varepsilon^p)$ are shown in Figure 7. The plots of main and total indices both show that $\mathrm{RMSD}(\varepsilon^p)$ is most sensitive to the parameters q and $\Delta\varphi_1$. Generally, the sensitivity to q starts from a lower value and rises with increasing strain, while sensitivity to $\Delta\varphi_1$ starts at a higher value and decreases for both T4 and T7 tempers. The most probable explanation is that as deformation develops and crystals rotate, activating multiple distinct slip systems, the interaction between slip systems becomes more important, while the small variation in the initial orientation and possible initial slip system activation becomes less important with increasing deformation. For the T4 temper at 15% strain, the sensitivity to q overtakes the sensitivity to $\Delta\varphi_1$. In contrast, for the T7 material the sensitivity to $\Delta\varphi_1$ is so high initially that it is still dominating even at 15% global strain, while the sensitivity to q at this strain level is still relatively small in comparison. The third most important material parameter is τ_1, which almost always has a significantly smaller sensitivity index than the first two. The total sensitivity indices of the other parameters are much higher than their main indices, meaning that their effects on the plastic strain field depend on the values of other parameters. The previous study on the latent hardening [19] indicates that if a more advanced latent hardening description was used, the variability of the stress-strain fields and their sensitivity to latent hardening could be even higher.

The main and total sensitivity indices for $\mathrm{RMSD}(\sigma)$, $\mathrm{RMSD}(P)$ and $\mathrm{RMSD}(T)$ exhibit the same trends as $\mathrm{RMSD}(\varepsilon^p)$ and are not shown here. The parameters $\Delta\varphi_1$ and q dominate, with $\Delta\varphi_1$ more important at small strains and for the T7 material. The initial slip resistance τ_0 is usually the third most important, except for the T7 material in the 2D model, where the parameter τ_1 sometimes takes its place.

Considering the mesh resolution influence on the uncertainty and sensitivity of the model response, the following argument can be made. The presented CPFEM model type was used

extensively in the literature. The convergence studies universally show that increasing mesh density improves the resolution of the mechanical fields but does not change the field "shape" significantly. An example of this may be found in [44]. The field gradients will become sharper, which should in principle increase RMSD of the corresponding fields.

5. Conclusions

UQSA methods were applied to study the variability and sensitivity of global and local solutions of a CP-FEM model to the variations in material model parameters. Both a 2D plane-strain model and a 3D model (using Voronoi tessellation) with 10 grains each were created, representing oligocrystals. Five sets of 10 random grain orientations were assigned to each oligocrystal. Two baseline material types were tested: a high work-hardening material based on the AA6063-T4 alloy, and a low work-hardening, high yield stress material based on the AA6063-T7 alloy. To investigate the effects of parameter variability on the predictions of model simulations, polynomial chaos expansions for outputs of interest representing the strain and stress fields and the global force were estimated. UQ measures and sensitivity indices were calculated from the polynomial chaos expansion. The generated stress and strain fields and the global force were analysed by normalizing them and comparing to the baseline fields and force. The results show that the equivalent plastic strain field may have significant variation, mostly due to early onset of strain localization. If the material work-hardening rate is high and the plastic flow is not constrained, then the variation of the plastic strain is quite low. The variation in the von Mises equivalent stress field is typically low, which means that it is possible to obtain a good estimate of the equivalent stress distribution in the oligocrystal even with uncertain values of the material parameters. On the other hand, the variations in the hydrostatic stress and stress triaxiality fields are significant, compared to the equivalent stress field and in some cases also the equivalent plastic strain field. The sensitivity study shows that the mechanical fields are most sensitive to the uncertainty in the crystallographic orientation and the latent hardening. The other parameters are mostly important in combination with each other. For the global force, in contrast, the strongest sensitivity index was obtained for the initial slip resistance. In the case of the low work-hardening material, the other parameters are almost irrelevant, while for the high work-hardening material they become somewhat more prominent for higher strains and in combination with each other. The correlation between the global force variation and the plastic strain field variation is very low, showing that the relationship between local and global solutions depends heavily on the material parameters.

Thus it is, in general, impossible to infer the local behaviour from global measurements without accurate knowledge of the material parameters.

The application of the UQSA to the CP-FEM models is challenging, because of the high computational cost of the CP-FEM models. Therefore, only five sets of orientations and models of oligocrystals were used in this study. Nevertheless, the results show consistent trends for all tested sets of crystallographic orientations, despite the fact that the orientations were all picked randomly from the whole orientation space. The CP-FEM solutions for the mechanical fields, such as the equivalent plastic strain field (which may be calculated by means of digital image correlation and used in various applications, e.g. material model calibration or fracture studies) and the hydrostatic pressure and stress triaxiality fields (which are crucial for advanced fracture predictions) show significant variability, due to uncertainty in the material parameters. The solution is most sensitive to the uncertainty in the Euler orientation angle and the latent hardening description. A similar UQSA study could be performed for specific polycrystal configurations and BCs tailored to a particular problem. Such a study would highlight and evaluate quantitatively the more particular trends relevant for that exact model.

Acknowledgements

Mikhail Khadyko, Odd Sture Hopperstad and Stéphane Dumoulin gratefully appreciate the financial support from NTNU and the Research Council of Norway through the FRINATEK Programme, Project No. 250553 (FractAl). Special thanks to Dr. V.G. Eck.

References

[1] Guery A, Hild F, Latourte F, Roux S. Slip Activities in Polycrystals Determined by Coupling Dic Measurements with Crystal Plasticity Calculations. *Int J Plasticity* 2016;81:249-266.

[2] Guery A, Latourte F, Hild F, Roux S. Identification of Crystal Plasticity Law Parameters Using Kinematic Measurements in Polycrystals, *WCCM XI-11th World Congress on Computational Mechanics*, 2014;8 pp.

[3] Heripre E, Dexet M, Crepin J, Gélebart L, Roos A, Bornert M, Caldemaison D. Coupling between Experimental Measurements and Polycrystal Finite Element Calculations for Micromechanical Study of Metallic Materials. *Int J Plasticity* 2007;23:1512-1539.

[4] Musienko A, Tatschl A, Schmidegg K, Kolednik O, Pippan R, Cailletaud G. Three-Dimensional Finite Element Simulation of a Polycrystalline Copper Specimen. *Acta Mater* 2007;55:4121-4136.

[5] Zhang C, Li H, Eisenlohr P, Liu W, Boehlert C, Crimp M, Bieler T. Effect of Realistic 3d Microstructure in Crystal Plasticity Finite Element Analysis of Polycrystalline Ti-5al-2.5 Sn. *Int J Plasticity* 2015;69:21-35.

[6] Pinna C, Lan Y, Kiu M, Efthymiadis P, Lopez-Pedrosa M, Farrugia D. Assessment of Crystal Plasticity Finite Element Simulations of the Hot Deformation of Metals from Local Strain and Orientation Measurements. *Int J Plasticity* 2015;73:24-38.

[7] Lim H, Carroll J, Battaile C, Buchheit T, Boyce B, Weinberger C. Grain-Scale Experimental Validation of Crystal Plasticity Finite Element Simulations of Tantalum Oligocrystals. *Int J Plasticity* 2014;60:1-18.

[8] Sachtleber M, Zhao Z, Raabe D. Experimental Investigation of Plastic Grain Interaction. *Mat Sci Eng* 2002;336:81-87.

[9] Hoc T, Crépin J, Gélébart L, Zaoui A. A Procedure for Identifying the Plastic Behavior of Single Crystals from the Local Response of Polycrystals. *Acta Mater* 2003;51:5477-5488.

[10] Saai A, Louche H, Tabourot L, Chang H. Experimental and Numerical Study of the Thermo-Mechanical Behavior of Al Bi-Crystal in Tension Using Full Field Measurements and Micromechanical Modeling. *Mechanics of Materials* 2010;42:275-292.

[11] Badulescu C, Grédiac M, Haddadi H, Mathias J-D, Balandraud X, Tran H-S. Applying the Grid Method and Infrared Thermography to Investigate Plastic Deformation in Aluminium Multicrystal. *Mechanics of Materials* 2011;43:36-53.

[12] Cuadra J, Baxevanakis K, Loghin A, Kontsos A. Validation of a Cyclic Plasticity Computational Method Using Fatigue Full‐Field Deformation Measurements. *Fatigue & Fracture of Engineering Materials & Structures* 2016.

[13] Zhang T, Jiang J, Britton B, Shollock B, Dunne F. Crack Nucleation Using Combined Crystal Plasticity Modelling, High-Resolution Digital Image Correlation and High-

Resolution Electron Backscatter Diffraction in a Superalloy Containing Non-Metallic Inclusions under Fatigue, *Proc. R. Soc. A*, 2016;472:20150792.

[14] Dumoulin S, Hopperstad OS, Sène NA, Balland P, Arrieux R, Moreau J-M. Numerical Modelling of Plastic Forming of Aluminium Single Crystals. *International Journal of Material Forming* 2013;6:13-27.

[15] Lim H, Abdeljawad F, Owen SJ, Hanks BW, Foulk JW, Battaile CC. Incorporating Physically-Based Microstructures in Materials Modeling: Bridging Phase Field and Crystal Plasticity Frameworks. *Model Simul Mater Sc* 2016;24:045016.

[16] Zeghadi A, Forest S, Gourgues A-F, Bouaziz O. Ensemble Averaging Stress–Strain Fields in Polycrystalline Aggregates with a Constrained Surface Microstructure–Part 2: Crystal Plasticity. *Philos Mag* 2007;87:1425-1446.

[17] Teodosiu C, Raphanel JL. Finite Element Simulations of Large Elastoplastic Deformations of Multicrystals, *Proceedings of the International Seminar MECAMAT91*, 1991;153-168.

[18] Needleman A, Asaro R, Lemonds J, Peirce D. Finite Element Analysis of Crystalline Solids. *Comput Method Appl M* 1985;52:689-708.

[19] Khadyko M, Dumoulin S, Cailletaud G, Hopperstad O. Latent Hardening and Plastic Anisotropy Evolution in Aa6060 Aluminium Alloy. *Int J Plasticity* 2016;76:51-74.

[20] Ghiocel DM, Ghanem RG. Stochastic Finite-Element Analysis of Seismic Soil–Structure Interaction. *Journal of Engineering Mechanics* 2002;128:66-77.

[21] Hall JW, Boyce SA, Wang Y, Dawson RJ, Tarantola S, Saltelli A. Sensitivity Analysis for Hydraulic Models. *Journal of Hydraulic Engineering* 2009;135:959-969.

[22] Fassò A, Cameletti M. A Unified Statistical Approach for Simulation, Modeling, Analysis and Mapping of Environmental Data. *Simulation* 2010;86:139-153.

[23] Eck VG, Donders WP, Sturdy J, Feinberg J, Delhaas T, Hellevik LR, Huberts W. A Guide to Uncertainty Quantification and Sensitivity Analysis for Cardiovascular Applications. *International Journal for Numerical Methods in Biomedical Engineering* 2016;32:e02755-n/a.

[24] Pardoen T. Numerical Simulation of Low Stress Triaxiality Ductile Fracture. *Computers & Structures* 2006;84:1641-1650.

[25] Chen P, Zabaras N. Uncertainty Quantification for Multiscale Disk Forging of Polycrystal Materials Using Probabilistic Graphical Model Techniques. *Comp Mater Sci* 2014;84:278-292.

[26] Wen B, Zabaras N. A Multiscale Approach for Model Reduction of Random Microstructures. *Comp Mater Sci* 2012;63:269-285.

[27] Kouchmeshky B, Zabaras N. Microstructure Model Reduction and Uncertainty Quantification in Multiscale Deformation Processes. *Comp Mater Sci* 2010;48:213-227.

[28] Zabaras N. An Information-Theoretic Multiscale Framework with Applications to Polycrystalline Materials. Cornell Univercity, Materials Process, Design and Control Laboratory (MPDC), 2010.

[29] Madrid PJ, Sulsky D, Lebensohn RA. Uncertainty Quantification in Prediction of the in-Plane Young's Modulus of Thin Films with Fiber Texture. *Journal of Microelectromechanical Systems* 2014;23:380-390.

[30] Salvati E, Korsunsky A. An Analysis of Macro-and Micro-Scale Residual Stresses of Type I, Ii and Iii Using Fib-Dic Micro-Ring-Core Milling and Crystal Plasticity Fe Modelling. *Int J Plasticity* 2017.

[31] Hiriyur B, Waisman H, Deodatis G. Uncertainty Quantification in Homogenization of Heterogeneous Microstructures Modeled by Xfem. *International Journal for Numerical Methods in Engineering* 2011;88:257-278.

[32] Stevens GN. Experiment-Based Validation and Uncertainty Quantification of Partitioned Models: Improving Predictive Capability of Multi-Scale Plasticity Models. Clemson University; Clemson, 2016.

[33] Chernatynskiy A, Phillpot SR, LeSar R. Uncertainty Quantification in Multiscale Simulation of Materials: A Prospective. *Annual Review of Materials Research* 2013;43:157-182.

[34] Pham M, Creuziger A, Iadicola M, Rollett A. Roles of Texture and Latent Hardening on Plastic Anisotropy of Face-Centered-Cubic Materials During Multi-Axial Loading. *J Mech Phys Solids* 2017;99:50-69.

[35] Renner E, Gaillard Y, Richard F, Amiot F, Delobelle P. Sensitivity of the Residual Topography to Single Crystal Plasticity Parameters in Berkovich Nanoindentation on Fcc Nickel. *Int J Plasticity* 2016;77:118-140.

[36] Sudret B. Global Sensitivity Analysis Using Polynomial Chaos Expansions. *Reliability Engineering & System Safety* 2008;93:964-979.

[37] Rodriguez-Fernandez M, Kucherenko S, Pantelides C, Shah N. Optimal Experimental Design Based on Global Sensitivity Analysis. *Computer Aided Chemical Engineering* 2007;24:63.

[38] Feinberg J, Langtangen HP. Chaospy: An Open Source Tool for Designing Methods of Uncertainty Quantification. *Journal of Computational Science* 2015;11:46-57.

[39] Hutchinson J. Bounds and Self-Consistent Estimates for Creep of Polycrystalline Materials. *P Roy Soc Lond A Mat* 1976;348:101-127.

[40] Tome C, Canova G, Kocks U, Christodoulou N, Jonas J. The Relation between Macroscopic and Microscopic Strain Hardening in Fcc Polycrystals. *Acta Metall Mater* 1984;32:1637-1653.

[41] Grujicic M, Batchu S. Crystal Plasticity Analysis of Earing in Deep-Drawn Ofhc Copper Cups. *J Mat Sci* 2002;37:753-764.

[42] Flanagan D, Belytschko T. A Uniform Strain Hexahedron and Quadrilateral with Orthogonal Hourglass Control. *International Journal for Numerical Methods in Engineering* 1981;17:679-706.

[43] Hallquist JO. Ls-Dyna Theory Manual. *Livermore software technology corporation* 2006.

[44] Khadyko M, Dumoulin S, Hopperstad O. Texture Gradients and Strain Localisation in Extruded Aluminium Profile. *Int. J Solids Struct* 2016;97:239-255.

[45] Pan J, Rice JR. Rate Sensitivity of Plastic Flow and Implications for Yield-Surface Vertices. *Int. J Solids Struct* 1983;19:973-987.

[46] Gambin W. Refined Analysis of Elastic-Plastic Crystals. *Int. J Solids Struct* 1992;29:2013-2021.

[47] Bunge HJ, Morris PR. Texture Analysis in Materials Science: Mathematical Methods. 1982.

[48] Kocks U, Brown T. Latent Hardening in Aluminum. *Acta Metall Mater* 1966;14:87-98.

[49] Franciosi P, Berveiller M, Zaoui A. Latent Hardening in Copper and Aluminium Single Crystals. *Acta Metall Mater* 1980;28:273-283.

[50] Liu M, Lu C, Tieu AK. Crystal Plasticity Finite Element Method Modelling of Indentation Size Effect. *Int. J Solids Struct* 2015;54:42-49.

[51] Erinosho T, Cocks A, Dunne F. Texture, Hardening and Non-Proportionality of Strain in Bcc Polycrystal Deformation. *Int J Plasticity* 2013;50:170-192.

[52] Hammersley J. Monte Carlo Methods. Springer Science & Business Media, 2013.

Tables

Table 1: Ranges of the material model parameters for the 2D and 3D structures.

Parameter	AA6063-T4	AA6063-T7
$\Delta\varphi_1$ (°)	-2…0…2	-2…0…2
τ_0 (MPa)	20…30…40	40…60…80
τ_1 (MPa)	17…26…35	6…9…12
θ_0 (MPa)	163…244…325	129…194…257
θ_1 (MPa)	8…12…16	1…2…3
q	1…1.5…2	1…1.5…2

Table 2: Elastic and rate sensitivity parameters of the crystal plasticity model.

c_{11}, MPa	c_{12}, MPa	c_{44}, MPa	$\dot{\gamma}_0$, s^{-1}	m
106430	60350	28210	0.010	0.005

Figures

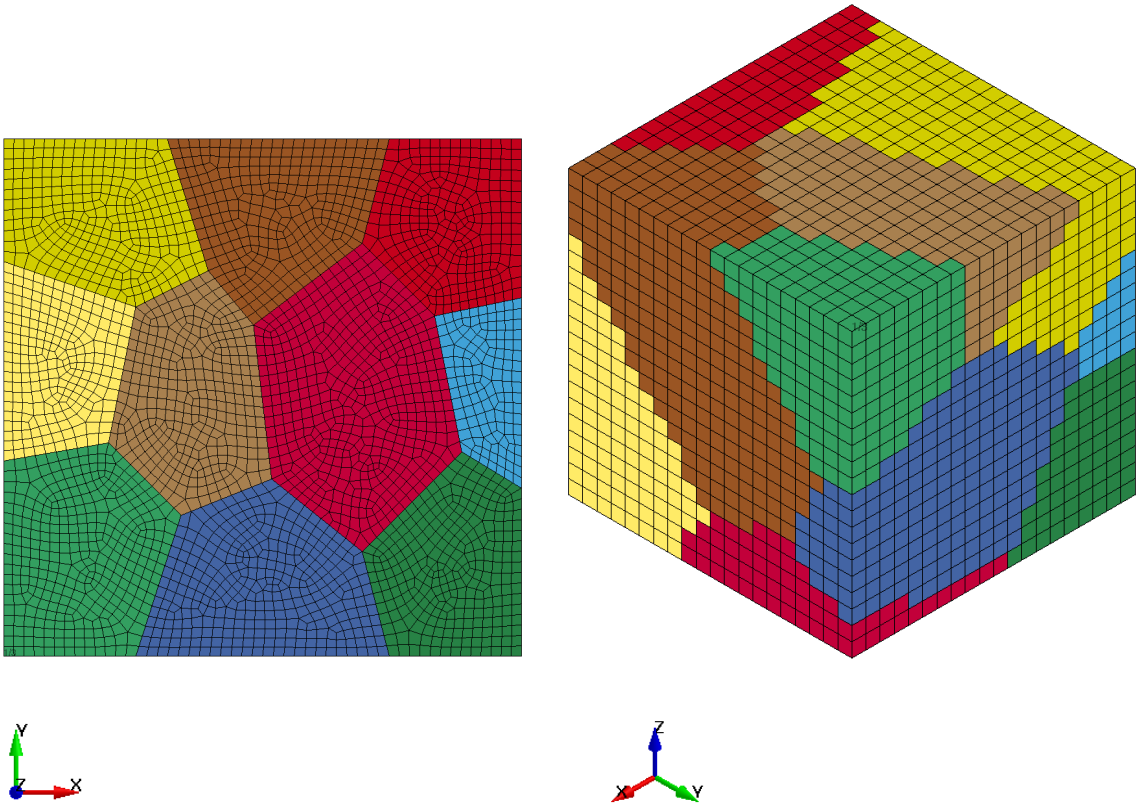

Figure 1: Illustrations of the 2D plane-strain and 3D microstructures.

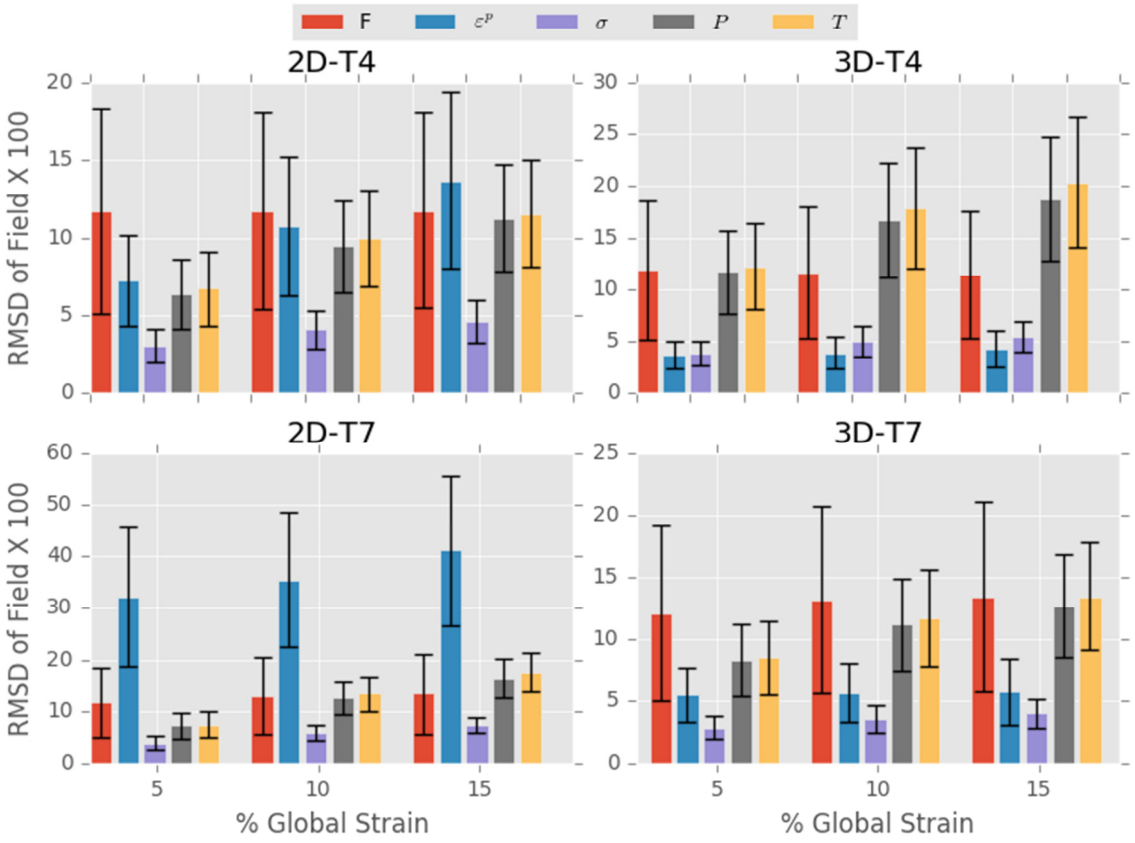

Figure 2: Root Mean Squared Deviation (see Equations (16) and (17)) for the outputs of interest. Bars represent the average expected value of RMSD across the 5 sets of crystallographic orientations considered, and the black error bars represent plus/minus the average standard deviation of RMSD across the orientations.

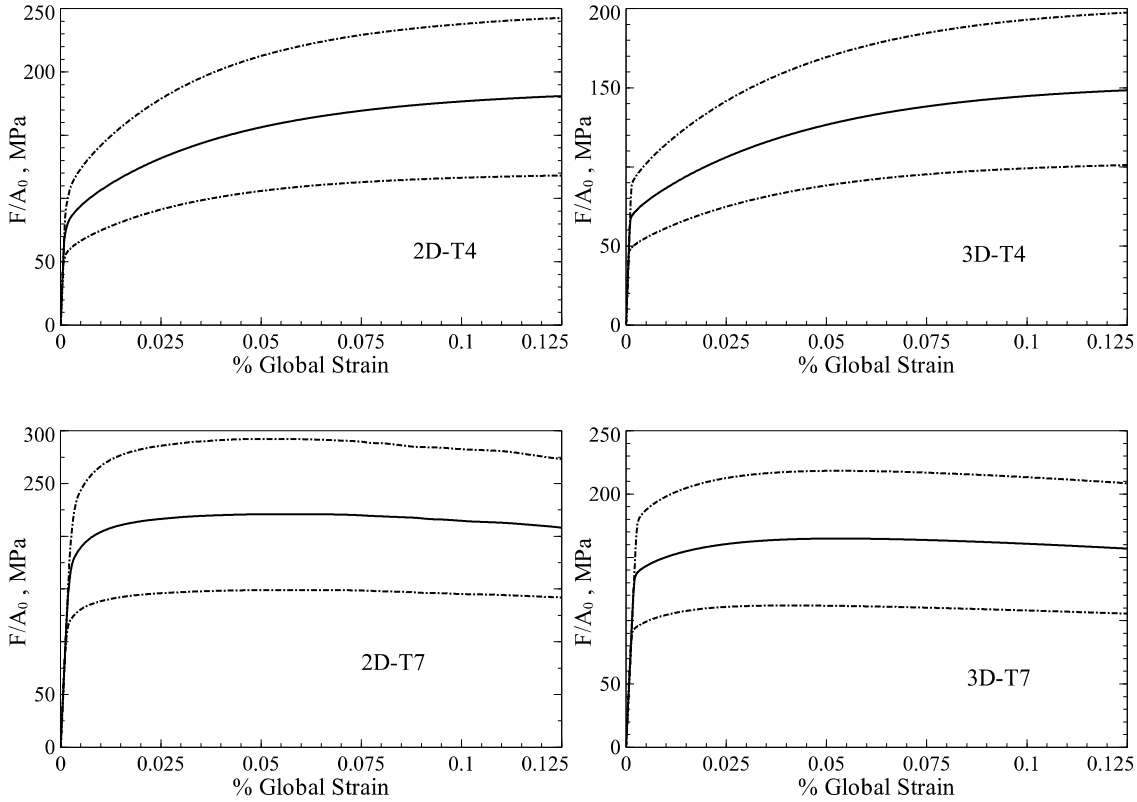

Figure 3: The engineering stress-strain curves of the baseline simulation (middle curve) and the simulations with the highest RMSD(F) (top and bottom curves) for one of the orientation sets.

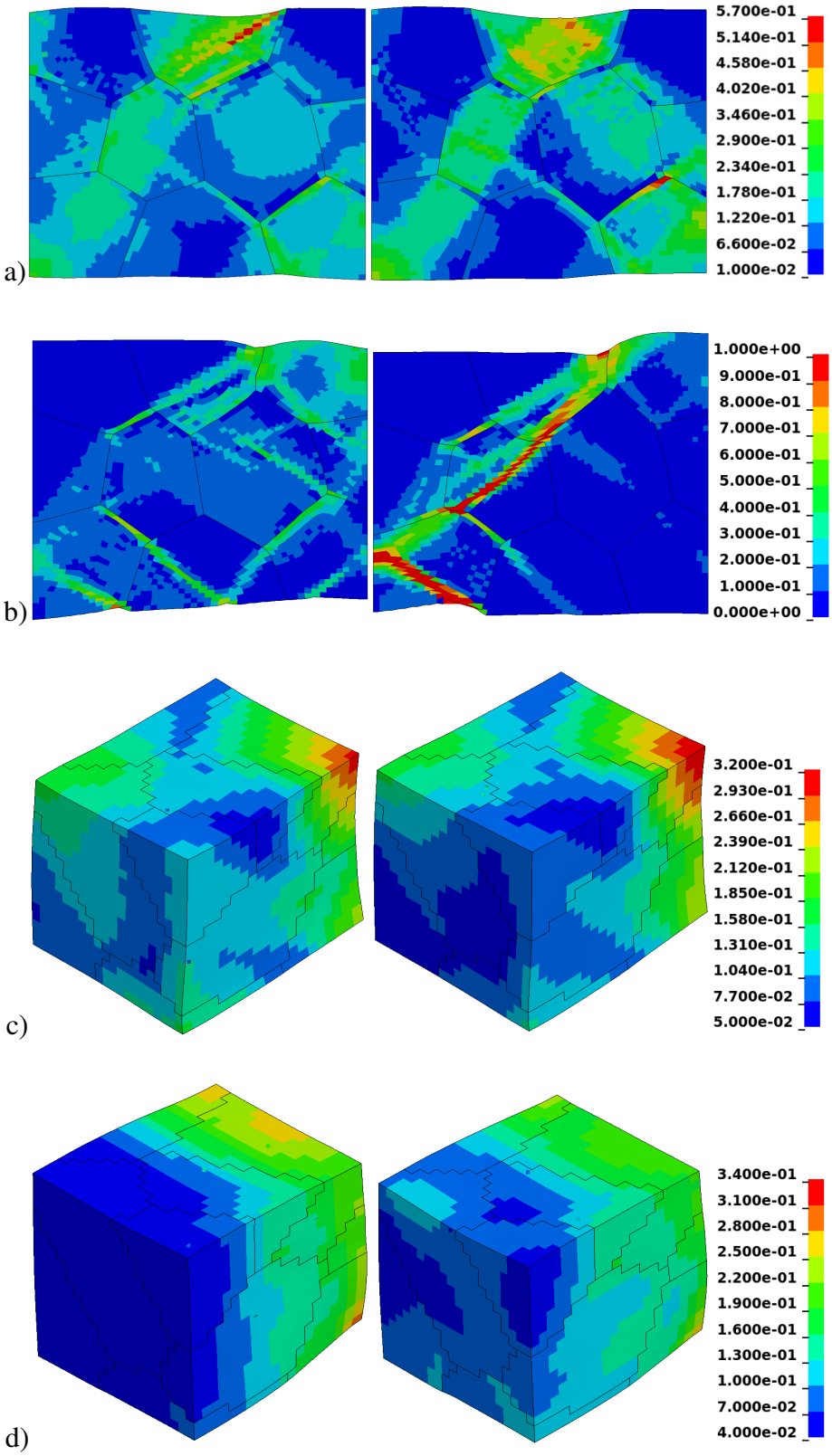

Figure 4: Equivalent plastic strain in the baseline simulation (left) and a simulation with the highest RMSD(ε^p) (right) for the a) 2D-T4, b) 2D-T7, c) 3D-T4 and d) 3D-T7 models.

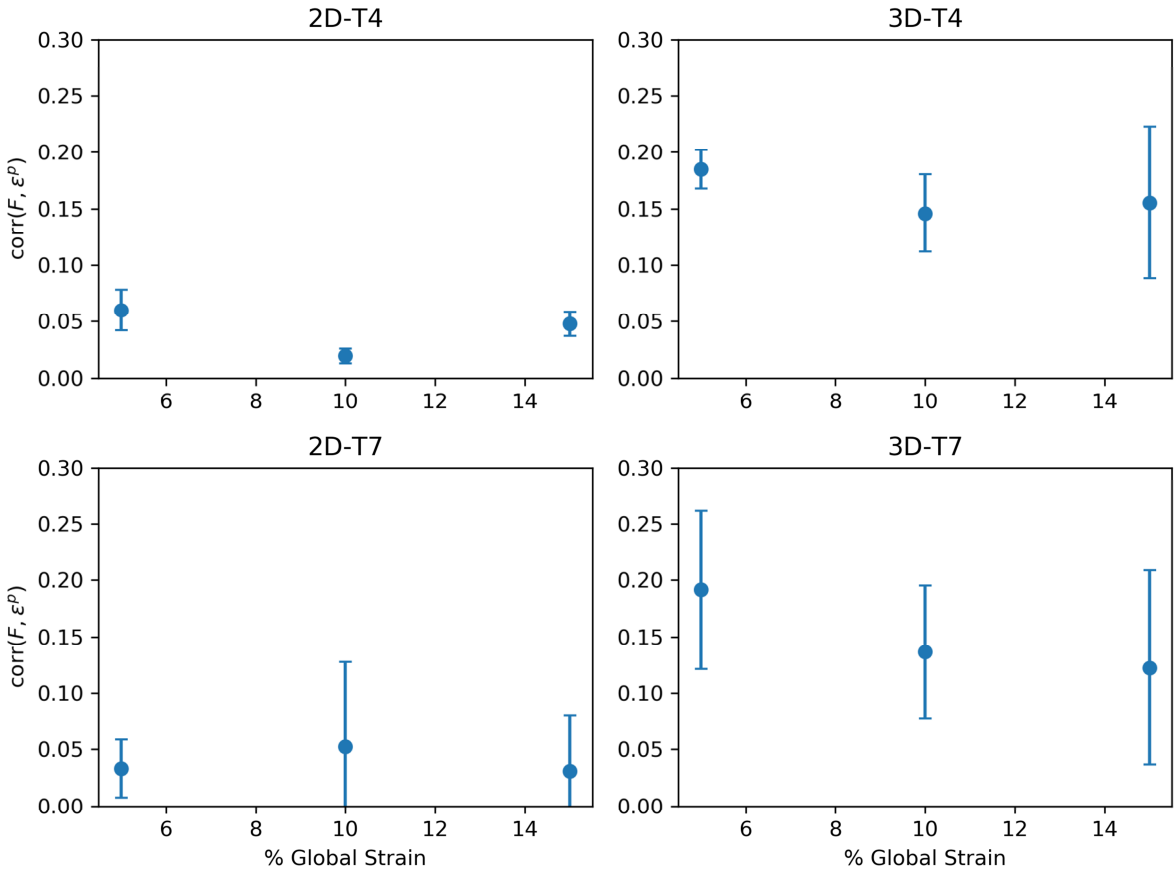

Figure 5: Sample correlation coefficient as defined in Equation (20) of the global force and plastic strain for the 5 models for each case between $\mathrm{RMSD}(F)$ and $\mathrm{RMSD}(\varepsilon^p)$. The points are the average value of the correlations and the error bars represent plus/minus one sample standard deviation of the correlation coefficients. The averages and standard deviations are determined according to Equation (20).

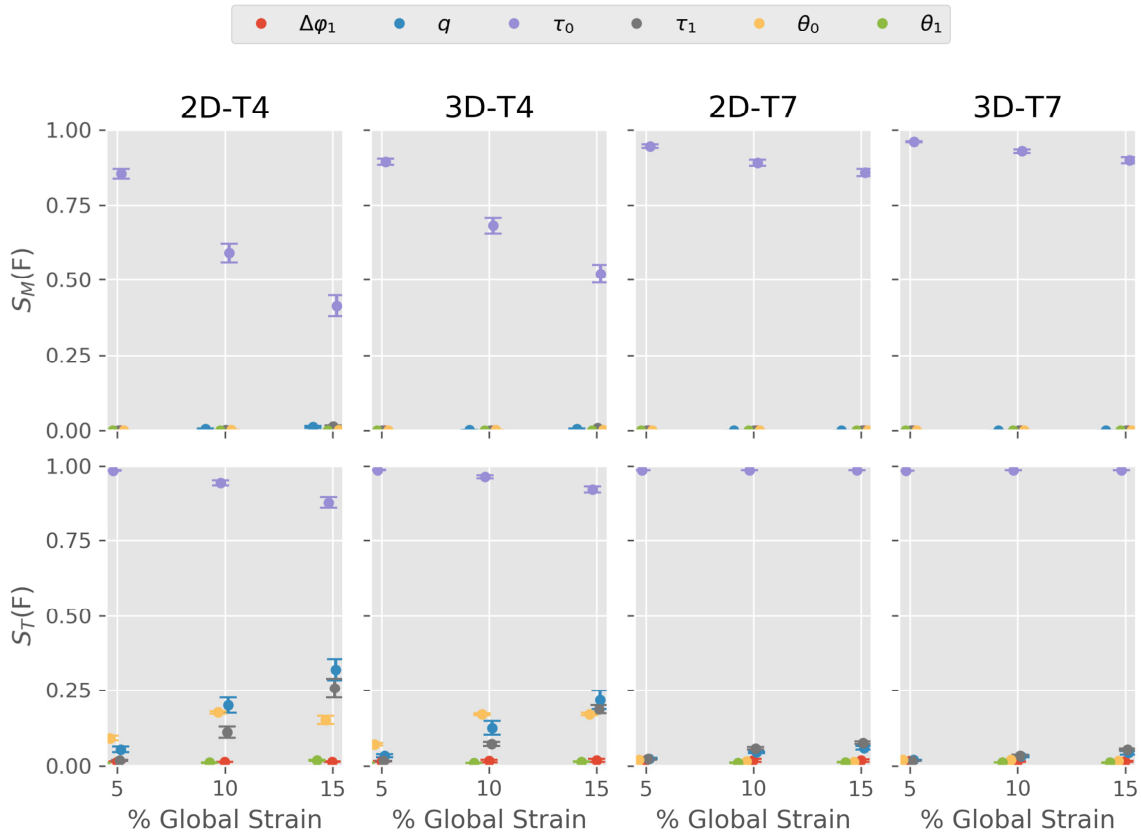

Figure 6: Main and total sensitivity indices S_M and S_T of the global force. Circles represent the average value of the sensitivity indices across the 5 sets of crystallographic orientations considered, and the error bars indicate plus/minus one standard deviation of the sensitivities across the orientations. For ease of viewing the x-position of the points is shifted by a small amount such that the sensitivities may be differentiated.

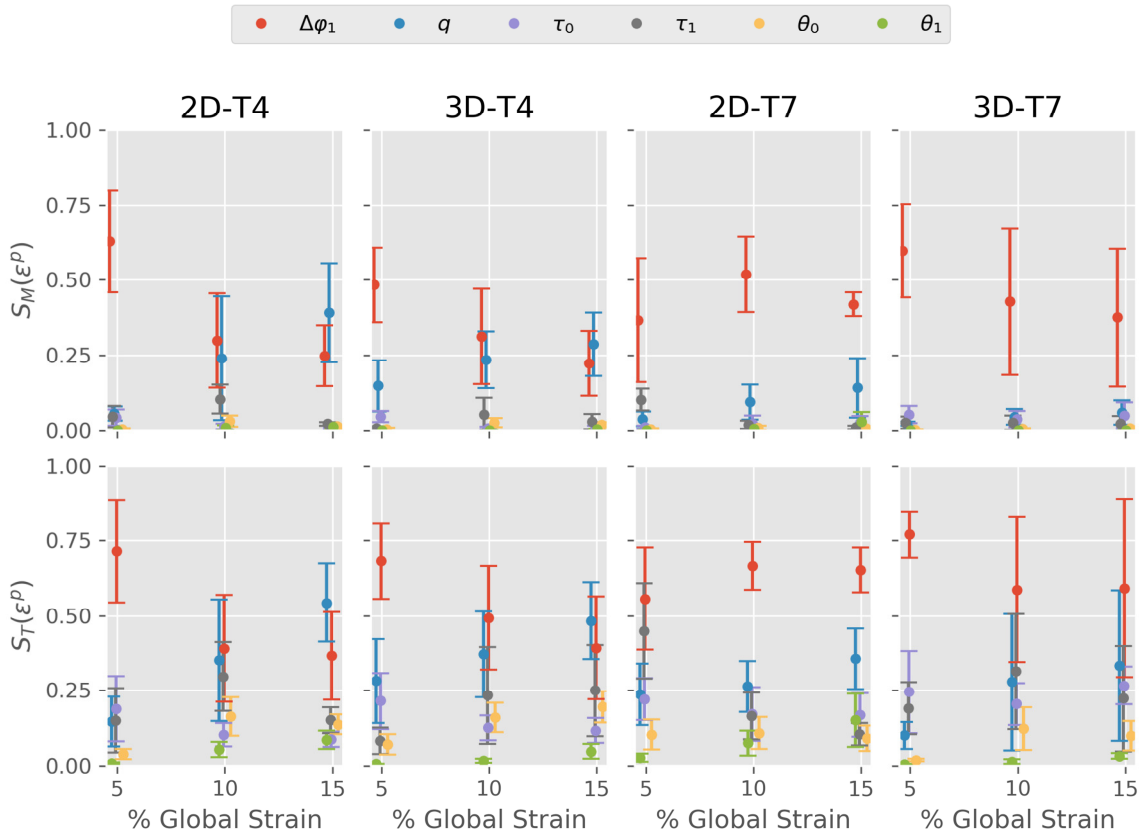

Figure 7: Main and total sensitivity indices S_M and S_T of the normalized equivalent plastic strain. Circles represent the average value of the sensitivity indices across the 5 sets of crystallographic orientations considered, and the error bars indicate plus/minus one standard deviation of the sensitivities across the orientations. For ease of viewing the x-position of the points is shifted by a small amount such that the sensitivities may be differentiated.